Journal of Alloys and Compounds 480 (2009) 558–563

Contents lists available at ScienceDirect

Journal of Alloys and Compounds

journal homepage: www.elsevier.com/locate/jallcom

Synthesis of HCP, FCC and BCC structure alloys in the Mg–Ti binary system by means of ball milling

Kohta Asano*, Hirotoshi Enoki, Etsuo Akiba

National Institute of Advanced Industrial Science and Technology (AIST), AIST Central-5, 1-1-1, Higashi, Tsukuba, Ibaraki 305-8565, Japan

ARTICLE INFO

Article history:
Received 10 December 2008
Received in revised form 19 January 2009
Accepted 25 January 2009
Available online 6 February 2009

Keywords:
Magnesium–titanium alloys
Crystal structure
Mechanical alloying
Ball milling
Hydrogen storage

ABSTRACT

Mg_xTi_{100-x} ($35 \le x \le 80$) alloys with hexagonal close packed (HCP), face centered cubic (FCC) and body centered cubic (BCC) structures were successfully synthesized by means of ball milling. Mg_xTi_{100-x} alloys with a BCC structure at $x = 35$ and 50 and with a HCP structure at $x = 80$ were synthesized by milling of Mg and Ti powder using stainless steel milling balls and pots. At $x = 65$, the BCC and HCP phases were synthesized. Mg_xTi_{100-x} alloys with a FCC structure were synthesized at $x = 35$ and 50 by milling using zirconia milling balls and pots. The FCC and HCP phases were synthesized at $x = 65$ and 80 using zirconia milling balls and pots. The crystal structure of Mg_xTi_{100-x} alloys synthesized by the ball milling method depended on the materials of milling balls and pots. That indicates that milling products are determined by the dynamic energy given by the milling setup. The lattice parameters of Mg_xTi_{100-x} in the HCP, FCC and BCC phases increased with increase of the Mg content, x.

1. Introduction

The mechanical alloying method such as ball milling has a potential for synthesizing novel materials. In the reported binary phase diagram of the Mg–Ti system, solubility of each metal to another is less than 2 at.% and intermetallic compounds are not found [1]. Synthesis of the Mg–Ti alloys by the melting methods has not been successful because the difference in melting points between Mg (923 K) and Ti (1943 K) is significant [1] and Mg markedly vaporizes during melting process. We have successfully synthesized Mg_xTi_{100-x} ($25 \le x \le 60$) alloys with a body centered cubic (BCC) structure by ball milling of Mg and Ti powder [2–5].

Plastic deformation and mix of raw materials are repeated in the ball milling process. Mg and Ti have a hexagonal close packed (HCP) structure at ambient temperatures. The principal plastic deformation modes of HCP metals are plane slips and twinning deformation [6]. The main slip systems in HCP metals are a $\{0001\}\langle\bar{1}2\bar{1}0\rangle$ basal plane slip system with a-axis slip direction and a $\{10\bar{1}0\}\langle\bar{1}2\bar{1}0\rangle$ prismatic plane slip system with a-axis slip direction [7]. Mg is deformed mainly by the basal plane slip at ambient temperatures. The value of the critical resolved shear stress (CRSS) of the basal plane slip system is about two orders magnitude smaller than that of the prismatic plane slip system [7]. In case of the deformation of Ti, the value of the CRSS of the basal plane slip system is slightly larger than that of the prismatic plane slip system [7]. Ti is deformed by the twinning deformation much more readily than Mg [6]. The main twinning deformation mode of Ti is a $\{11\bar{2}2\}$ twinning below 573 K and a $\{10\bar{1}1\}$ twinning in combination with a $\langle c+a\rangle$ slip above 673 K [8,9].

In our previous work [5], the synthesis process of Mg–Ti BCC alloys in ball milling was studied by X-ray diffraction (XRD) and microscopic techniques. During ball milling of Mg and Ti powder, Mg and Ti were deformed mainly by the basal plane slip and the twinning deformation, respectively. Mg dissolved in Ti and the metastable BCC phase was synthesized.

Liang and Schulz [10] have synthesized Mg_xTi_{100-x} ($x \ge 80$) HCP alloys by means of ball milling. Borsa et al. [11] have synthesized Mg_xTi_{100-x} ($55 < x < 95$) thin films with a HCP structure by co-sputtering of Mg and Ti. Kalisvaart and Notten [12] have synthesized Mg_xTi_{100-x} ($65 \le x \le 85$) alloys by means of ball milling which consisted of two face centered cubic (FCC) phases. The crystal structure of metastable Mg_xTi_{100-x} alloys seems to depend on the synthesis methods and the ratio of Mg and Ti.

The present work aims to synthesize various crystal structures of Mg_xTi_{100-x} alloys by controlling ball milling conditions and the ratio of Mg and Ti. Our concept is that the crystal structure of milled products is closely related to the plastic deformation process of raw materials during ball milling. The compressive stress to the raw materials should be affected by the dynamic energy given by the milling balls, *i.e.*, the mass of milling balls. The powder of Mg and Ti has been milled using stainless steel and zirconia milling balls in order to change the power to give powders.

* Corresponding author. Tel.: +81 29 861 4410; fax: +81 29 861 4410.
E-mail address: k.asano@aist.go.jp (K. Asano).

0925-8388/$ – see front matter © 2009 Elsevier B.V. All rights reserved.
doi:10.1016/j.jallcom.2009.01.086

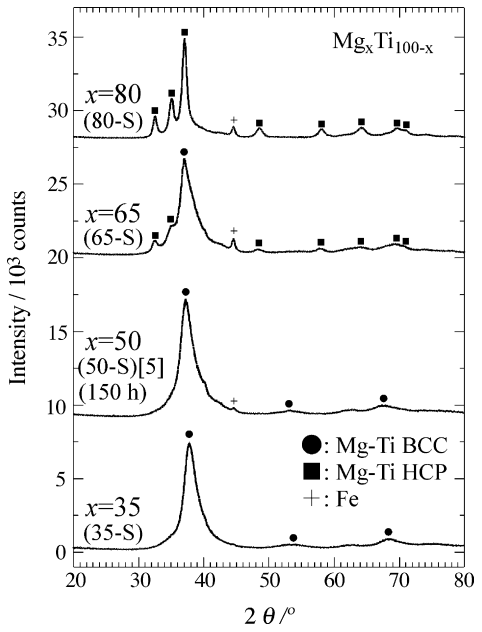

Fig. 1. X-ray diffraction patterns of Mg_xTi_{100-x} (x = 35, 50 [5], 65 and 80) alloys milled for 200 h using stainless steel milling balls and pots.

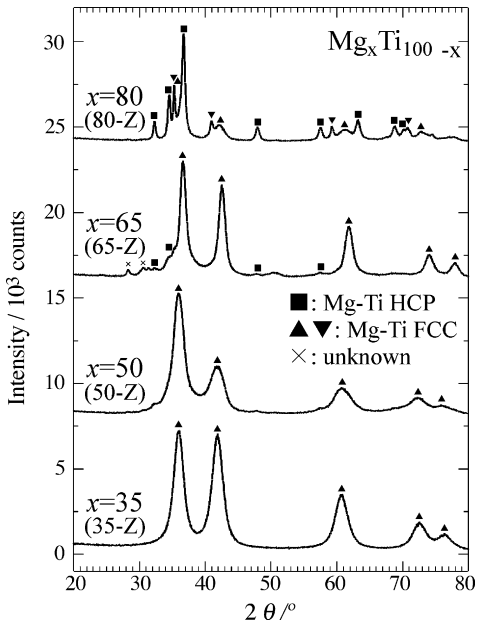

Fig. 2. X-ray diffraction patterns of Mg_xTi_{100-x} (x = 35, 50, 65 and 80) alloys milled for 200 h using zirconia milling balls and pots.

2. Experimental

The powder of Mg (<150 μm, 99.9 mass%) purchased from Furuuchi Chemical and Ti (<45 μm, 99.9 mass%) purchased from Wako Pure Chemical was weighed in a globe box filled with purified argon. Metal powder and milling balls with a diameter of 10 mm were set in milling pots. The milling balls and pots made of stainless steel and zirconia were used and the internal volumes of stainless steel and zirconia pots were 140 cm^3 and 80 cm^3, respectively. The total amount of metal powder was 1–2 g. The ball milling was performed using a Fritsch P5 planetary ball mill for 50–200 h. The rotation speed was fixed at 200 rpm.

The powder X-ray diffraction (XRD) was measured using a Rigaku 2500 V diffractometer with Cu Kα radiation. The lattice parameter of the alloys was calculated from the XRD peak positions and the crystallite size from the width of the diffraction peaks by using of Scherrer's equation [13], respectively. Chemical analysis was performed by an EDAX Genesis2000 energy dispersive X-ray spectrometer (EDX). Morphology of the alloys was observed by a JEOL JEM-2000FX II transmission electron microscope (TEM). The pressure differential scanning calorimetry (PDSC) curves of the Mg_xTi_{100-x}–H_2 system were measured under a hydrogen pressure of 4.5 MPa in the temperature range from 323 K to 773 K with the heating and cooling rate of 5 K min^{-1} using a Rigaku DSC8230HP. Hydrogen gas of 7N purity was used.

3. Results and discussion

In our previous work [2,3], ball milling of Mg and Ti powder with various atomic ratios was performed in an argon atmosphere for 200 h using stainless steel milling balls and pots. The BCC phase was synthesized at the chemical composition of x = 25, 33, 50 and 60 in Mg_xTi_{100-x}. At x = 50, the lattice parameter was calculated to be a = 0.342(1) nm and the crystallite size to be 3 nm [5]. In the Mg-rich composition at x = 67 and 75, Mg and Ti significantly stuck on the surface of milling balls and pots and the BCC phase was not found. In the present work, the total amount of Mg and Ti powder was reduced compared to the previous one (2 g) [2–5] in the Mg-rich composition at x = 65 and 80 in order to avoid sticking of metal powder. The alloys were removed from the surface of milling balls and pots after milling.

Fig. 1 shows the XRD patterns of Mg_xTi_{100-x} (x = 35, 50 [5], 65 and 80) alloys milled for 200 h using stainless steel milling balls and pots. Mg_xTi_{100-x} (x = 35, 50, 65 and 80) alloys synthesized by stainless steel milling balls and pots were designated as 35-S, 50-S, 65-S and 80-S, respectively, in order to distinguish them from the other products milled using zirconia milling balls and pots. As shown in Fig. 1, small peaks of Fe were observed in the XRD patterns of the 50-S, 65-S and 80-S. However, Fe was not detected by the EDX measurement and the exact content of Fe could not be determined. The product 35-S was the BCC phase. The previous result showed that the BCC phase was synthesized in the region of x = 25–60 [2,3]. On the other hand, in the XRD pattern of the 80-S the HCP phase was observed and the lattice parameters were determined to be a = 0.317(7) nm and c = 0.513(9) nm. These lattice parameters are between Mg (a = 0.32094 nm, c = 0.52105 nm) and Ti (a = 0.2951 nm, c = 0.46843 nm) [14]. The crystallite size of the HCP phase synthesized was estimated to be 15 nm from the width of the diffraction peaks. Both the HCP and BCC phases were observed in the XRD pattern of the 65-S.

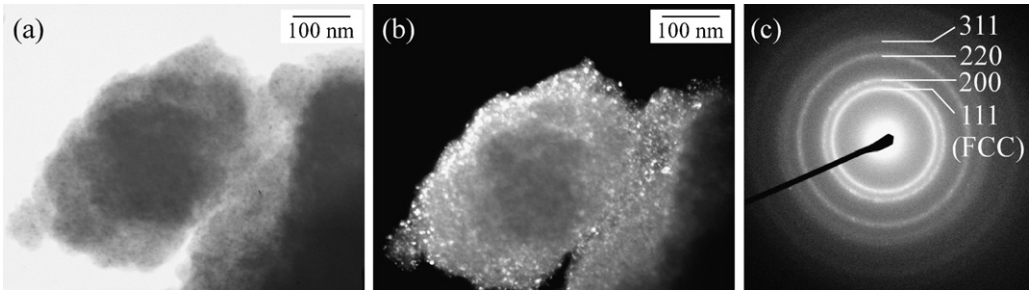

Fig. 3. Transmission electron microscope images of $Mg_{50}Ti_{50}$ FCC alloy (50-Z); (a) bright-field, (b) dark-field and (c) SAD images.

Table 1
Crystal structure, lattice parameter and crystallite size of Mg_xTi_{100-x} alloys.

	x in Mg_xTi_{100-x}	Milling balls and pot	Synthesized phase structure	Lattice parameter (nm)		Crystallite size (nm)
				a	c	
35-S	35	Stainless steel	BCC	0.338(1)	–	3
50-S [5]	50	Stainless steel	BCC	0.342(1)	–	3
65-S	65	Stainless	HCP	0.317(5)	0.515(6)	>6
		steel	BCC	0.342(0)	–	>3
80-S	80	Stainless steel	HCP	0.317(7)	0.513(9)	15
35-Z	35	Zirconia	FCC	0.430(5)	–	5
50-Z	50	Zirconia	FCC	0.431(7)	–	5
65-Z	65	Zirconia	HCP	0.319(3)	0.520(1)	>10
			FCC	0.423(8)	–	>7
80-Z	80	Zirconia	HCP	0.319(1)	0.518(9)	19
			FCC	0.427(2)	–	>5
			FCC	0.438(8)	–	>4

Fig. 2 shows the XRD patterns of Mg_xTi_{100-x} (x = 35, 50, 65 and 80) alloys milled for 200 h using zirconia milling balls and pots. Mg_xTi_{100-x} (x = 35, 50, 65 and 80) alloys synthesized by zirconia milling balls and pots were designated as 35-Z, 50-Z, 65-Z and 80-Z, respectively. In the XRD patterns of the 35-Z and 50-Z, the FCC phase was observed. The lattice parameter and the crystallite size of the 50-Z were estimated to be a = 0.431(7) nm and 5 nm, respectively. Fig. 3(a)–(c) show the TEM images of the 50-Z; (a) bright-field, (b) dark-field and (c) selected area electron diffraction (SAD) images. The crystallite size of the 50-Z was smaller than 10 nm but the exact mean crystallite size could not be determined from Fig. 3(a) and (b) because boundaries of the crystallites were not clear. The SAD image in Fig. 3(c) exhibits a series of co-axial rings which correspond to the FCC structure. The lattice parameter was calculated to be a = 0.43(4) nm from the radii of diffraction rings and this value agrees well with a = 0.431(7) nm determined from XRD data. As shown in Fig. 2, the HCP phase was observed in the XRD pattern of the 80-Z. That is similar to the 80-S shown in Fig. 1. The product of the 80-Z consisted of not only the HCP phase but also two FCC phases which have different lattice parameters a = 0.427(2) nm and 0.438(8) nm. In the XRD pattern of the 65-Z, the FCC phase was observed in addition to slight amount of the HCP phase. The crystal structural data of Mg_xTi_{100-x} alloys synthesized by the present work was summarized in Table 1. The crystal structure and lattice parameter of Mg_xTi_{100-x} alloys depend upon the chemical composition and the material of milling balls.

The schematic drawing of planetary ball milling is shown in Fig. 4. The acceleration of milling balls during ball milling, g, is expressed by Eq. (1) [15]

$$g = \left(r_{\mathrm{rev}} - \frac{r_{\mathrm{p}}^2 (1 + R_{\mathrm{rat}})^2}{r_{\mathrm{rev}}} \right) \left(\frac{2\pi R_{\mathrm{rev}}}{60} \right)^2 \quad (1)$$

where r_{rev} is the revolution radius of milling pots and r_{p} is the radius of milling pots. R_{rev} is the revolution speed of milling pots and R_{rat} is the ratio of rotation speed to revolution speed of milling pots. The masses, m, of stainless steel and zirconia balls were 4.2 g and 3.2 g, respectively. The radius, r_{p}, of a stainless steel pot was 37 mm and that of a zirconia pot was 33 mm. The kinetic energy of a moving ball at collision to the surface of a milling pot, E, can be estimated using Eq. (2)

$$E = \frac{m(gt)^2}{2} \quad (2)$$

where t is time between removal of a ball from the surface of a milling pot and collision to the surface. The value, E, of a zirconia ball was around 70% of that of a stainless steel ball at R_{rev} = 200 rpm.

The milling time dependence of the XRD patterns of (a) 50-S [5], (b) 80-S and (c) 50-Z is shown in Fig. 5(a)–(c). In the XRD pattern of the 50-S in Fig. 5(a), diffraction peaks of the BCC phase and Ti were observed in addition to small peaks of Mg after 100 h milling. The diffraction peaks of Ti were broadened. It has been indicated by XRD and observation of the milled product by a scanning electron microscope that Ti transformed from the HCP phase to the BCC phase by solution of Mg into Ti during ball milling [5]. In the XRD pattern of the 80-S shown in Fig. 5(b), diffraction peaks of Ti disappeared and those of Mg shifted to higher angle. This XRD result indicates that Ti randomly dissolved in Mg without changing the crystal structure. In the XRD pattern of the 50-Z shown in Fig. 5(c), after 50 h milling, the intensity of diffraction peaks of Mg and Ti reduced and the FCC phase was observed. The most intense peak that is 1 1 1 diffraction peak of the FCC phase overlaps with 0 0 2 diffraction peak of Mg and 1 0 0 diffraction peak of Ti.

FCC and HCP structures are the closest packing one composed a stack of the closest packing planes. The closest packing plane in the FCC structure is {1 1 1} plane and the primary slip system in FCC metals is known to be a {1 1 1}⟨1 1 0⟩ plane slip system [16]. On the assumption that {0 0 0 1} basal plane slip in Mg and $\{10\bar{1}0\}$ prismatic plane slip in Ti with a HCP structure generate {1 1 1}

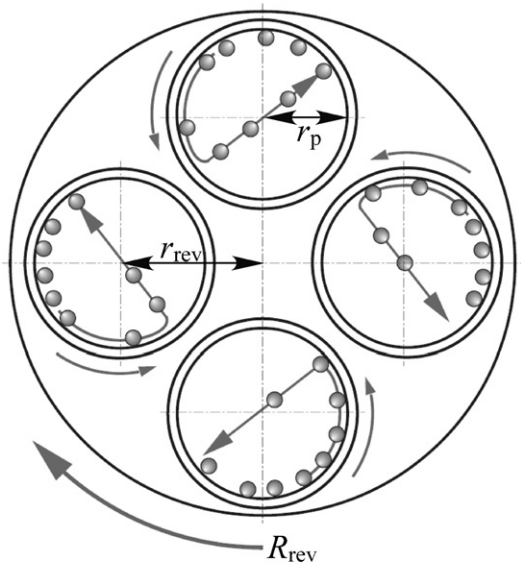

Fig. 4. Schematic drawing of planetary ball milling.

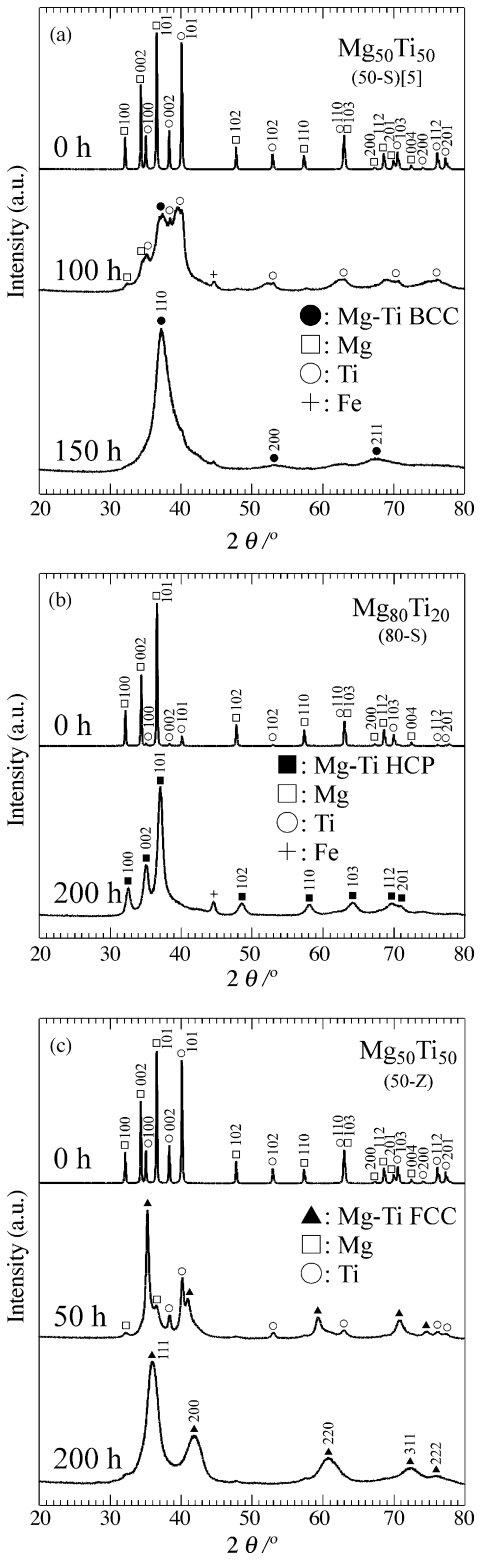

Fig. 5. X-ray diffraction patterns of (a) $Mg_{50}Ti_{50}$ BCC (50-S) [5], (b) $Mg_{80}Ti_{20}$ HCP (80-S) and (c) $Mg_{50}Ti_{50}$ FCC (50-Z) alloys milled for 0–200 h.

plane of the Mg–Ti FCC phase, numbers of stacking faults should be introduced into Mg and Ti during milling.

Fadeeva et al. [17] have reported that Al dissolved in Ti by milling of Ti and Al powder and the HCP solid solution phase of Ti and Al was formed. The HCP lattice of the Ti–Al solid solution was distorted due to introduction of numbers of dislocations by milling.

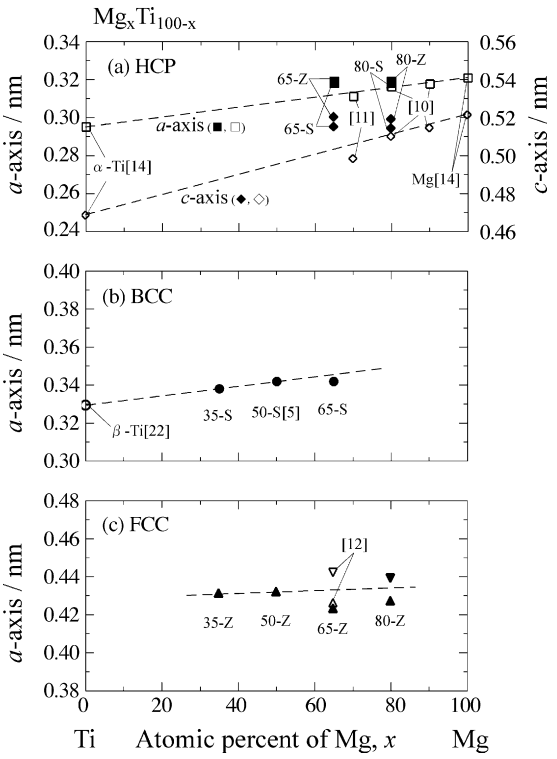

Fig. 6. Lattice parameters of (a) HCP, (b) BCC and (c) FCC phases of Mg_xTi_{100-x} alloys.

Stacking faults were formed by gliding of the dislocations introduced on the basal and prismatic planes in the HCP lattice. By annealing of $Ti_{50}Al_{50}$ HCP alloy after milling, the HCP phase transformed to the metastable FCC phase [17]. The FCC crystals were coherent to the HCP ones and {1 1 1} plane of the FCC phase was parallel to {0 0 0 1} plane of the HCP phase [17]. In case of the Mg–Ti system, we assume that the FCC phase observed in Fig. 2 was also formed by introduction of stacking faults in a HCP structure of Mg and Ti. According to the calculations of the stacking fault energy (SFE) and the twin boundary energy (TBE) in HCP metals [9,18], the value of the SFE is comparable to that of the TBE in Mg ($\{11\bar{2}2\}$ SFE: 173 mJ m^{-2}, $\{1\,1\,\bar{2}\,2\}$ TBE: 186 mJ m^{-2}) and Ti ($\{11\bar{2}2\}$ SFE: 357 mJ m^{-2}, $\{11\bar{2}2\}$ TBE: 488 mJ m^{-2}). The stacking faults which are associated with dissociation of the dislocations are similar in stability to twin boundaries in both Mg and Ti [9].

In the present work, the FCC phase was synthesized using zirconia milling balls and the BCC phase using stainless steel ones. The density of stacking faults introduced by milling in the BCC phase is speculated to be higher than that in the FCC phase because the dynamic energy given by stainless steel balls during milling was higher than that by zirconia ones. In case of stainless and carbon steels, a FCC structure transforms to a BCC structure by the strain-induced nucleation which is due to introduction of stacking faults [19,20]. The difference in crystal structures between the BCC and FCC phases in Mg–Ti alloys should be related to the density of stacking faults. Indeed, the crystallite size that is sensitive to the density of stacking faults was 3 nm in the BCC phase of the 50-S [5] and was 5 nm in the FCC phase of the 50-Z.

Fig. 6(a)–(c) show lattice parameters of (a) HCP, (b) BCC and (c) FCC phases of Mg_xTi_{100-x} alloys. The lattice parameters of the three phases increased with increase of x because Mg has larger atomic radius compared to Ti. The lattice parameters of the HCP phase of the 80-S, Mg [14] and Ti [14] were followed by Vegard's law [21] shown a dotted line in Fig. 6(a). However, the lattice parameters of the HCP phase of the 65-S, the 65-Z and the 80-Z were found above the line in Fig. 6(a). The 65-S consisted of the BCC and HCP

phases, the 65-Z of the FCC and HCP phases and the 80-Z of the HCP and two FCC phases, respectively. The lattice parameters of the BCC phase of the 35-S, the 50-S [5] and β-Ti [22] were also followed by Vegard's law [21] as shown in Fig. 6(b). The lattice parameter of the BCC phase of the 65-S was slightly below the line. Kalisvaart and Notten [12] synthesized Mg_xTi_{100-x} ($65 \le x \le 85$) alloys by means of ball milling. The alloys consisted of two FCC phases. The lattice parameters of the two FCC phases at $x = 65$ were $a = 0.426$ nm and $a = 0.442$ nm [12] that is also shown in Fig. 6(c). Kalisvaart and Notten [12] reported that the lattice parameter depended on the composition, *i.e.*, the smaller FCC phase was Ti-rich and the larger one was Mg-rich. The compositions of the HCP and BCC phases in the 65-S were considered to be Mg-rich and Ti-rich. The lattice parameters of the FCC phase in the 65-Z was slightly smaller than the linear relationship of the 35-Z and the 50-Z in Fig. 6(c). The HCP and FCC phases in the 65-Z were Mg-rich and Ti-rich, respectively. Considering the lattice parameter of each phase in the 80-Z, the Mg-rich HCP, Mg-rich larger FCC and Ti-rich smaller FCC phases were formed.

The PDSC curves of the 80-S, the 50-Z and the 50-S [4] under a hydrogen pressure of 4.5 MPa with the heating and cooling rate of 5 K min^{-1} are shown in Fig. 7. Several exothermic peaks around 550–720 K and one endothermic peak around 740 K were observed in the heating run for every alloy. In the cooling run, one exothermic peak around 720 K was observed. In our previous work [4], the $Mg_{42}Ti_{58}H_{177}$ FCC hydride phase was synthesized from $Mg_{50}Ti_{50}$ BCC alloy under a hydrogen pressure of 8 MPa at 423 K. It has been

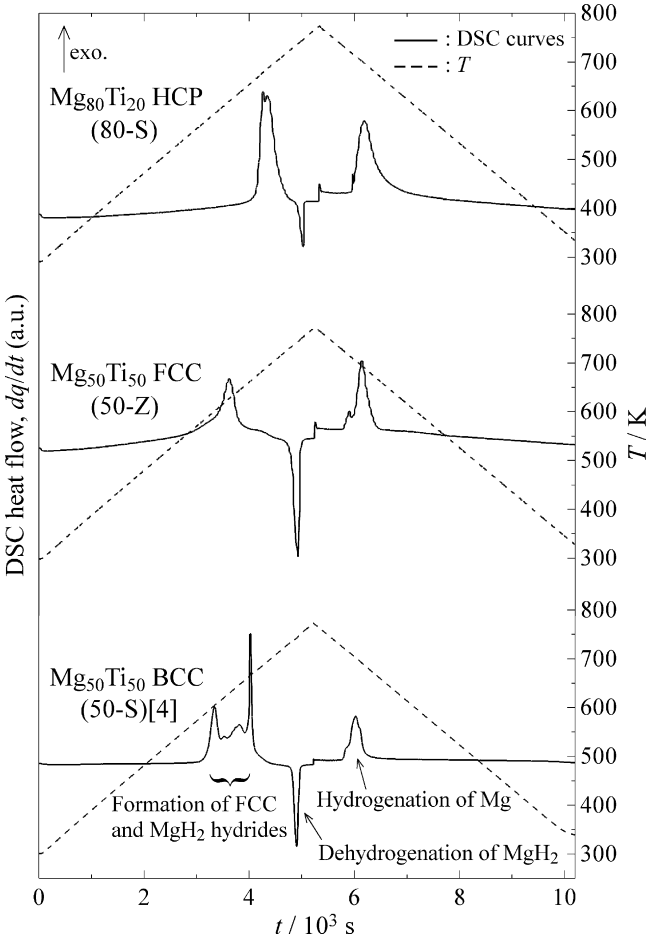

Fig. 7. Pressure differential scanning calorimetry curves of $Mg_{80}Ti_{20}$ HCP (80-S), $Mg_{50}Ti_{50}$ FCC (50-Z) and $Mg_{50}Ti_{50}$ BCC (50-S) [4] alloys with heating and cooling rate of 5 K min^{-1} under a hydrogen pressure of 4.5 MPa.

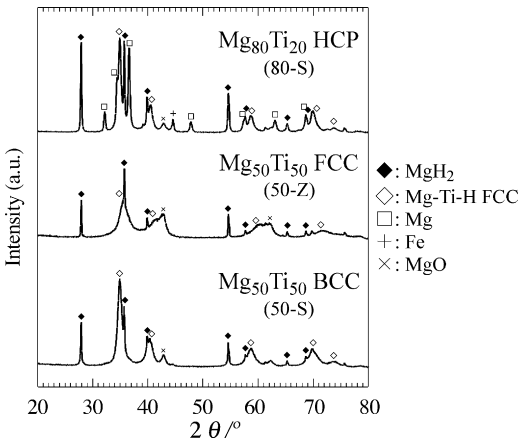

Fig. 8. X-ray diffraction patterns of $Mg_{80}Ti_{20}$ HCP (80-S), $Mg_{50}Ti_{50}$ FCC (50-Z) and $Mg_{50}Ti_{50}$ BCC (50-S) alloys after pressure differential scanning calorimetry measurements.

identified that the endothermic peak in the heating run of the 50-S was attributed to the dehydrogenation of MgH_2 by comparing the measured peak temperature with the dehydrogenation temperature estimated using van't Hoff equation [4]. The exothermic peaks in the heating run were attributed to formation of the FCC and MgH_2 hydride phases from the $Mg_{50}Ti_{50}$ BCC phase [4]. In the cooling run, the exothermic peak was attributed to the hydrogenation of Mg [4].

Fig. 8 shows the XRD patterns of the 80-S, the 50-Z and the 50-S after the PDSC measurements. Every alloy was partially oxidized during the PDSC measurements and diffraction peaks of MgO oxide were observed. The FCC and MgH_2 hydride phases were formed in the 80-S and the 50-Z as well as the 50-S. The exothermic peaks in the heating run of the 80-S and the 50-Z shown in Fig. 7 were also attributed to formation of the FCC and MgH_2 hydride phases. Hydrogenation of the 50-S and the 50-Z is speculated to proceed readily compared to that of the 80-S because the exothermic peak temperatures of the 50-S and the 50-Z were lower than that of the 80-S in the heating run. In the diffraction pattern of the 80-S shown in Fig. 8, the peaks of the Mg phase were also observed. The Mg content of the 80-S was overabundant for formation of the FCC hydride phase and excess Mg was segregated. The phase abundance of the FCC hydride phase in the 50-Z was lower than that in the 50-S because the phase abundance of the MgO phase in the 50-Z was high compared to that in the 50-S. Consequently, the intensity of XRD peaks of the FCC phase in the 50-Z was lower than that in the 50-S.

4. Conclusions

Mg and Ti powder with various atomic ratios was milled using stainless steel and zirconia milling balls and pots. Mg_xTi_{100-x} ($35 \le x \le 80$) alloys which consisted of the HCP, FCC and BCC phases were successfully synthesized. The HCP phase was formed by solution of Ti into Mg and the BCC phase by solution of Mg into Ti. The FCC phase was stabilized by introduction of stacking faults in Mg and Ti which have a HCP structure.

Acknowledgement

The authors would like to thank Dr. H. Shao of National Institute of Advanced Industrial Science and Technology (AIST) for his valuable discussion. This work is supported by The New Energy and Industrial Technology Development Organization (NEDO) under "Development for Safe Utilization and Infrastructure of Hydrogen".

References

[1] A.A. Nayeb-Hashemi, J.B. Clark, Phase Diagrams of Binary Magnesium Alloys, 1988, p. 324.
[2] Y. Tsushio, S.J. Choi, H. Enoki, E. Akiba, Japanese Patent No. P2003-253360A.
[3] Y. Tsushio, S.J. Choi, H. Enoki, E. Akiba, Collected Abstracts of the 2002 Spring Meeting of the Japan Inst. Metals, 2002, p.499.
[4] K. Asano, H. Enoki, E. Akiba, J. Alloys Compd., doi:10.1016/j.jallcom.2008.11.019, in press.
[5] K. Asano, H. Enoki, E. Akiba, Acta Mater., submitted for publication.
[6] M.H. Yoo, Metall. Trans. A 12 (1981) 409.
[7] H. Tonda, S. Ando, Metall. Mater. Trans. A 33 (2002) 831.
[8] N.E. Paton, W.A. Backofen, Metall. Trans. 1 (1970) 2839.
[9] M.H. Yoo, J.R. Morris, K.M. Ho, S.R. Agnew, Metall. Mater. Trans. A 33A (2002) 813.
[10] G. Liang, R. Schulz, J. Mater. Sci. 38 (2003) 1179.
[11] D.M. Borsa, R. Gremaud, A. Baldi, H. Schreuders, J.H. Rector, B. Kooi, P. Vermeulen, P.H.L. Notten, B. Dam, R. Griessen, Phys. Rev. B 75 (2007) 205408.
[12] W.P. Kalisvaart, P.H.L. Notten, J. Mater. Res. 23 (2008) 2179.
[13] H.P. Klug, L.E. Alexander, X-ray Diffraction Procedures 2nd ed., Mellon Institute of Science, Carnegie-Mellon University, 1974, p. 656.
[14] Metal Databook Ver. 3, Japan Institute of Metals, 1993 (in Japanese).
[15] Operating Instructions of Fritsch Planetary Mill “pulverisette 5”.
[16] C.N. Reid, Deformation Geometry for Materials Scientists, International Series on Materials Science and Technology, vol. 11, Pergamon Press, 1973, p. 105.
[17] V.I. Fadeeva, A.V. Leonov, E. Szewczak, H. Matyja, Mater. Sci. Eng. A 242 (1998) 230.
[18] Y. Minonishi, S. Ishioka, M. Koiwa, S. Morozumi, M. Yamaguchi, Philos. Mag. A 43 (1981) 1017.
[19] G.B. Olson, M. Cohen, J. Less-Common Met. 28 (1972) 107.
[20] C.W. Sinclair, R.G. Hoagland, Acta Mater. 56 (2008) 4160.
[21] L. Vegard, Z. Phys. 5 (1921) 17.
[22] S.D. Smith, J. Inst. Met. 81 (1952–1953) 73.